

Angle-resolved photoemission in doped charge-transfer Mott insulators

A.S. Alexandrov and C. J. Dent

Department of Physics, Loughborough University, Loughborough LE11 3TU, U.K.

A theory of angle-resolved photoemission (ARPES) in doped cuprates and other charge-transfer Mott insulators is developed taking into account the realistic (LDA+U) band structure, (bi)polaron formation due to the strong electron-phonon interaction, and a random field potential. In most of these materials the first band to be doped is the oxygen band inside the Mott-Hubbard gap. We derive the coherent part of the ARPES spectra with the oxygen hole spectral function calculated in the non-crossing (ladder) approximation and with the exact spectral function of a one-dimensional hole in a random potential. Some unusual features of ARPES including the polarisation dependence and spectral shape in $\text{YBa}_2\text{Cu}_3\text{O}_7$ and $\text{YBa}_2\text{Cu}_4\text{O}_8$ are described without any Fermi-surface, large or small. The theory is compatible with the doping dependence of kinetic and thermodynamic properties of cuprates as well as with the d-wave symmetry of the superconducting order parameter.

PACS numbers:74.20.Mn,74.20.-z,74.25.Jb

1. Introduction

The concept of polarons led to the discovery of the copper oxide superconductors. The expectation was that if ‘an electron and a surrounding lattice distortion with a high effective mass can travel through the lattice as a whole, and a strong electron-phonon coupling exists, the perovskite insulator could be turned into a high temperature superconductor’¹. In this paper we develop the theory of ARPES in doped charge-transfer Mott insulators based on the bipolaron theory^{2,3} which describes some unusual ARPES features of high- T_c $\text{YBa}_2\text{Cu}_3\text{O}_{7-\delta}$ (Y123), $\text{YBa}_2\text{Cu}_4\text{O}_8$ (Y124) and a few other materials.

ARPES data in cuprates remains highly controversial⁴. One of the surprising features is a *large* Fermi surface claimed to exist in a wide range of doping fitting well the LDA band structures in the earlier studies. This should evolve with doping as $(1-x)$ in a clear contradiction with low frequency kinetics and thermodynamics (see, for example⁵⁻¹⁰, which show an evolution proportional to x in a wide range of doping including the overdoped region^{9,11} (x is the number of holes introduced by doping). Now it is established, however, that there is a normal state (pseudo)gap in ARPES and tunnelling, existing well above T_c ^{12,13}, so that some segments of a ‘large Fermi surface’ are actually missing¹⁴. The temperature and doping dependence of the gap still remain a subject of controversy. While kinetic⁹, thermodynamic¹⁰, tunnelling¹³ and some ARPES^{14,15} data suggest that the gap opens at any relevant temperature in a wide range of doping, other ARPES studies¹⁷⁻¹⁹ claim that it exists only in underdoped samples below a characteristic

temperature T^* .

Perhaps the most intriguing feature of ARPES is the extremely narrow and intense peak lying below the Fermi energy, which is most clearly seen near the Y and X points in Y124²⁰, Y123²¹ and more recently in $\text{La}_{2-x}\text{Sr}_x\text{CuO}_4$ ²². Its angular dependence and spectral shape as well as the origin of the featureless (but dispersive) background remain unclear. Some authors²⁰ refer to the peak as an extended van Hove singularity (evHs) arising from the plane (CuO_2) strongly correlated band. They also implicate the resulting (quasi)1D density of states singularity as a possible origin for the high transition temperature. However, recent polarised ARPES studies of untwinned Y123 crystals of exceptional quality²¹ unambiguously refer the peak to as a narrow resonance arising primarily from the quasi-1D CuO_3 chains in the buffer layers rather than from the planes. Also, careful analysis of the Eliashberg equations shows that the van Hove singularity can hardly be the origin of high T_c , in sharp contrast with a naive weak-coupling estimate. Interestingly, a very similar narrow peak was observed by Park *et al*²³ in high-resolution ARPES near the gap edge of the cubic *semiconductor* FeSi with no Fermi surface at all.

In this paper we take the view that cuprates and many other transition metal compounds are charge transfer Mott-Hubbard insulators at *any* level of doping²⁴. This means that the first band to be doped is the oxygen band lying within the Hubbard gap, Fig.1. Strong coupling with high frequency phonons, unambiguously established for many oxides²⁵, leads to the high-energy spectral features of an oxygen hole in an energy window about twice the Franck-Condon (polaronic) level shift, E_p , and to the band-narrowing effect². On the other hand, the low energy spectral function is influenced by the low frequency thermal lattice, spin and random fluctuations. The latter can be described as ‘Gaussian white noise’. The p -hole polaron in oxides is almost one-dimensional due to a large difference in the $pp\sigma$ and $pp\pi$ hopping integrals and effective ‘one-dimensional’ localisation by the random potential as described in Ref.²⁶. This allows us to explain the narrow peak in the ARPES spectra with the spectral density $A(k, E)$ of a one-dimensional particle in a Gaussian white noise potential²⁷.

The electron-phonon interaction also binds holes into inter-site oxygen bipolarons the size of a lattice constant^{2,28}. The bipolaron density remains relatively low (below 0.15 per cell) at any relevant level of doping. The residual repulsive (Coulomb) polaron-bipolaron interaction² is strongly suppressed by the lattice polarisation owing to a large static dielectric constant. As

a result, the only role of hole bipolarons in ARPES is to pin the chemical potential inside the charge transfer gap, half the bipolaron binding energy above the oxygen band edge, Fig.1a. This binding energy as well as the singlet-triplet bipolaron exchange energy are thought to be the origin of the normal state pseudogaps, as first proposed by one of us²⁹. In particular, the non-Korringa temperature dependence of NMR²⁹, and more recently the values and universal scaling with temperature of the uniform magnetic susceptibility^{30,6,31} and electronic specific heat³¹ were quantitatively described with bipolarons. In overdoped samples the bipolaron and polaron bands might overlap because the bipolaron binding energy becomes small³⁰, so the chemical potential might enter the oxygen band, Fig.1b, and then a Fermi-level crossing might be seen in ARPES. The featureless background is explained as the phonon cloud of a small hole polaron, which spreads over a wide energy interval about $2E_p \simeq 1eV$.

The same approach has been applied to the tunnelling spectra³². As a result, the temperature independent gap and the anomalous gap/T_c ratio, injection/emission asymmetry both in magnitude and shape, zero-bias conductance at zero temperature, the spectral shape inside and outside the gap region, temperature/doping dependence and dip-hump structure of the tunnelling conductance were described. The approach is compatible with the recent ‘LDA+U’ band structures in cuprates and manganites³³, which suggest the single-particle density of states shown in Fig.1. It is clearly compatible with the doping evolution of thermodynamic and kinetic properties because holes introduced by doping into the oxygen band are the only carriers in our theory. Moreover, the derived *bipolaron* energy dispersion with minima at the Brillouin zone boundaries provides *d*-wave symmetry of the Bose-Einstein condensate³² in agreement with phase-sensitive experiments³⁴. It also provides a parameter-free expression for T_c in a few dozen cuprates, irrespective of the level of doping^{35,36}.

Here we first derive the polaronic ARPES theory in Section 2. Then, in Section 3 we apply the simplest non-crossing approximation for the self-energy and compare it with the exact result in Section 4. The experimental ARPES results, in particular the angular dispersion, spectral shape and polarisation dependence are compared with the theory in Section 5. We conclude that the narrow peak in ARPES is an *intrinsic* polaron (oxygen) band found below the chemical potential by half of the bipolaron binding energy. We also arrive at the conclusion that the present experimental photoemission spectra can be understood with a small or even *without any* Fermi surface (depending on doping).

2. Polaronic ARPES

The interaction of the crystal with the electromagnetic field of frequency ν is described by the Hamiltonian (in the dipole approximation)

$$H_{int} = (8\pi I)^{1/2} \sin(\nu t) \sum_{\mathbf{k}, \mathbf{k}'} (\mathbf{e} \cdot \mathbf{d}_{\mathbf{k}, \mathbf{k}'}) c_{\mathbf{k}}^\dagger h_{\mathbf{k}'}^\dagger + H.c., \quad (1)$$

where I is the intensity of the radiation with the polarisation \mathbf{e} (we take $c = \hbar = k_B = 1$), \mathbf{k} is the momentum of the final state (i.e. of the photoelectron registered by the detector), \mathbf{k}' is the (quasi)momentum of the hole remaining in the sample after the emission, and $c_{\mathbf{k}}^\dagger$ and $h_{\mathbf{k}'}^\dagger$ are their creation operators, respectively. For simplicity we suppress the band index in $h_{\mathbf{k}'}^\dagger$. Due to the translational symmetry of the Bloch states, $|\mathbf{k}' \rangle \equiv u_{-\mathbf{k}'}(\mathbf{r}) \exp(-i\mathbf{k}' \cdot \mathbf{r})$, there is a momentum conservation rule in the dipole matrix element,

$$\mathbf{d}_{\mathbf{k}, \mathbf{k}'} = \mathbf{d}(\mathbf{k}) \delta_{\mathbf{k}+\mathbf{k}', \mathbf{G}} \quad (2)$$

with

$$\mathbf{d}(\mathbf{k}) = ie(N/v_0)^{1/2} \nabla_{\mathbf{k}} \int_{v_0} e^{-i\mathbf{G} \cdot \mathbf{r}} u_{\mathbf{k}-\mathbf{G}}(\mathbf{r}) d\mathbf{r}, \quad (3)$$

where \mathbf{G} is a reciprocal lattice vector, N the number of unit cells in the crystal of the volume Nv_0 .

The Fermi Golden Rule gives the photocurrent to be

$$I(\mathbf{k}, E) = 4\pi^2 I |\mathbf{e} \cdot \mathbf{d}(\mathbf{k})|^2 \times \sum_{i, f} e^{\Omega + \mu N_i - E_i} | \langle f | h_{\mathbf{k}-\mathbf{G}}^\dagger | i \rangle |^2 \delta(E + E_f - E_i), \quad (4)$$

where E is the binding energy, $E_{i, f}$ is the energy of the initial and final states of the crystal, and Ω, μ, N_i are the thermodynamic and chemical potentials and the number of holes, respectively. By definition the sum in Eq.(4) is $n(E)A(\mathbf{k}-\mathbf{G}, -E)$ where the spectral function $A(\mathbf{k}-\mathbf{G}, E) = (-1/\pi) \Im G^R(\mathbf{k}-\mathbf{G}, E)$ is proportional to the imaginary part of the retarded Green function (GF), and $n(E) = [\exp(E/T) + 1]^{-1}$, the Fermi distribution. In the following we consider temperatures well below the experimental energy resolution, so that $n(E) = 1$ if E is negative and zero otherwise, and, for convenience, we put $\mathbf{G} = 0$.

The spectral function depends on essential interactions of a single hole with the rest of the system. As we argued earlier²⁶ the most important interaction in oxides is the Fröhlich long-range electron-phonon interaction of the oxygen hole with the c-axis polarised high-frequency phonons. The Fröhlich interaction is integrated out with the Lang-Firsov canonical transformation³⁷. With the Quantum-Monte-Carlo technique³⁸ one can prove that this transformation is practically exact for a long-range interaction in a wide region of the coupling strength, including the intermediate and weak-coupling regime and in a wide range of the adiabatic ratio, ω/D (ω is the phonon frequency and D is the bandwidth). By applying the Lang-Firsov canonical transformation the hole Matsubara GF is expressed as a convolution of the coherent polaron GF and the multiphonon correlation function $\sigma(\mathbf{m}, \Omega_n)^3$,

$$\mathcal{G}(\mathbf{k}, \omega_n) = \frac{T}{N} \sum_{\omega_{n'}, \mathbf{m}, \mathbf{k}'} \frac{\sigma(\mathbf{m}, \omega_{n'} - \omega_n) e^{i(\mathbf{k} - \mathbf{k}') \cdot \mathbf{m}}}{i\omega_{n'} - \xi_{\mathbf{k}'}} \quad (5)$$

where the multi-phonon correlation function, $\sigma(\mathbf{m}, \tau) = T \sum_n e^{-i\Omega_n \tau} \sigma(\mathbf{m}, \Omega_n)$ is found as

$$\sigma(\mathbf{m}, \tau) = \exp\left(\frac{1}{2N} \sum_{\mathbf{q}} |\gamma(\mathbf{q})|^2 f_{\mathbf{q}}(\mathbf{m}, \tau)\right). \quad (6)$$

Here

$$f_{\mathbf{q}}(\mathbf{m}, \tau) = [\cos(\mathbf{q} \cdot \mathbf{m}) \cosh(\omega_{\mathbf{q}} |\tau|) - 1] \coth \frac{\omega_{\mathbf{q}}}{2T} + \cos(\mathbf{q} \cdot \mathbf{m}) \sinh(\omega_{\mathbf{q}} |\tau|)$$

with \mathbf{m} the lattice vector, $\omega_n = \pi T(2n + 1)$, $n = 0, \pm 1, \pm 2, \dots$ and $\Omega_n = 2\pi T n$.

In the case of dispersionless phonons and a short-range (Holstein) interaction with a q -independent matrix element ($\omega_{\mathbf{q}} = \omega$, $|\gamma(\mathbf{q})|^2 = 2g^2$) one can readily calculate the Fourier component of $\sigma(\mathbf{m}, \tau)$ to obtain³

$$\mathcal{G}(\mathbf{k}, \omega_n) = \frac{e^{-g^2}}{i\omega_n - \xi_{\mathbf{k}}} + \frac{e^{-g^2}}{N} \sum_{l=1}^{\infty} \frac{g^{2l}}{l!} \times \sum_{\mathbf{k}'} \left(\frac{n_{\mathbf{k}'}}{i\omega_n - \xi_{\mathbf{k}'} + l\omega} + \frac{1 - n_{\mathbf{k}'}}{i\omega_n - \xi_{\mathbf{k}'} - l\omega} \right). \quad (7)$$

The Green's function of a polaronic carrier comprises two different contributions. The first coherent \mathbf{k} -dependent term arises from the polaron band tunneling. The spectral weight of the coherent part is strongly (exponentially) suppressed as $Z = \exp(-g^2)$ and the effective mass is strongly enhanced, $\xi_{\mathbf{k}} = Z E_{\mathbf{k}} - \mu$ (we include the polaronic level shift into the chemical potential, μ). Here $E(\mathbf{k})$ is the bare (LDA+U) *hole* band dispersion. The second \mathbf{k} -independent contribution describes the excitations accompanied by the emission and absorption of phonons. We believe that this term, $I_{incoh}(E)$ is responsible for the asymmetric background in the optical conductivity and in the photoemission spectra of cuprates and manganites. We notice that its spectral density spreads over a wide energy range of about twice the polaron level shift $E_p = g^2 \omega$. On the contrary the coherent term shows an angular dependence in the energy range of the order of the polaron bandwidth $2w \equiv ZD$.

As we have discussed above ARPES measures the imaginary part of the retarded GF multiplied by the Fermi-Dirac distribution function and by the square of the dipole matrix element. G^R is obtained from $\mathcal{G}(\mathbf{k}, \omega_n)$ with a substitution $i\omega_n \rightarrow E + i0^+$. As a result we obtain

$$I(\mathbf{k}, E) \sim |d(\mathbf{k})|^2 n(E) Z \delta(E + \xi_{\mathbf{k}}) + I_{incoh}(E), \quad (8)$$

where $I_{incoh}(E)$ is a structureless function of the binding energy, which spreads from about $-\omega$ down to $-2E_p$. Only in the extreme limit of a very strong electron-phonon coupling, where the polaron bandwidth is well below the phonon frequency, can multiphonon structure

in $I_{incoh}(E)$ be verified. It has actually been observed in the optical conductivity²⁵.

The small Holstein polaron is very heavy except if the phonon frequency is extremely high²⁶. In fact, oxides are ionic semiconductors where the long-range electron-phonon interaction dominates. That leads to a much lighter mobile small Fröhlich polaron (SFP)^{26,38}. Considering the electron-phonon interaction in a multi-polaron system one has to take into account the dynamic properties of the dielectric response function³⁹. One can naively believe⁴⁰ that the long-range Fröhlich interaction becomes short range (Holstein) due to screening. This is of course untrue. In the long-wave limit ($q \rightarrow 0$) the response of polarons at the optical phonon frequency is dynamic, because $\omega \gg qv$ (v is the characteristic group velocity of polarons). Therefore, the singular (Fröhlich) behaviour of $\gamma(\mathbf{q}) \sim 1/q$ is unaffected by the screening. Polarons are slow enough and *cannot* screen the high-frequency crystal field oscillations. Hence, the interaction with the high-frequency optical phonons in ionic polaron solids remains long-range whatever the carrier density. It is easy to show⁴¹ using Eq.(5) and Eq.(6) that for any finite-radius interaction with a q -dependent matrix element the coherent part of ARPES spectra takes the same form as Eq.(8), but with a *different* spectral weight (Z) and effective mass (Z') renormalisation exponents. Also some \mathbf{k} dependence of the *incoherent* background appears if the matrix element of the electron-phonon interaction depends on q ⁴². Hence, in general,

$$I(\mathbf{k}, E) \sim |d(\mathbf{k})|^2 n(E) Z \delta(E + \xi_{\mathbf{k}}) + I_{incoh}(\mathbf{k}, E), \quad (9)$$

with the same $Z = \exp(-E_p/\omega)$ as in the case of the Holstein polaron but with the SFP bandwidth much less reduced, $\xi_{\mathbf{k}} = Z' E(\mathbf{k}) - \mu$, where $Z' = \exp(-\gamma E_p/\omega)$. In general one finds

$$\gamma = \sum_{\mathbf{q}} |\gamma(\mathbf{q})|^2 [1 - \cos(\mathbf{q} \cdot \mathbf{a})] / \sum_{\mathbf{q}} |\gamma(\mathbf{q})|^2, \quad (10)$$

and $E_p = (1/2) \sum_{\mathbf{q}} |\gamma(\mathbf{q})|^2 \omega_{\mathbf{q}}$. The numerical coefficient γ might be as small as 0.4 ³⁸ and even smaller in the cuprates with the nearest neighbour oxygen-oxygen distance less than the lattice constant, $\gamma \simeq 0.2$ ²⁶, which is precisely confirmed by exact QMC calculation of the small polaron mass³⁸. On the one hand this important result tells us that small polarons as well as intersite bipolarons are perfectly mobile and can account for the high- T_c values in cuprates³⁵. On the other the coherent spectral weight remains strongly suppressed in polaronic conductors, Eq.(9), because Z might be less than Z' by one or even a few orders of magnitude. These unusual SFP spectral features provide an explanation for the apparent discrepancy between a very small Drude weight and a relatively moderate mass enhancement, $m^* \sim 3m_e - 10m_e$ (depending on doping) of carriers in manganites^{43,44} and cuprates. They also explain why the evHs observed in ARPES²⁰⁻²² can be hardly seen in angle averaged photoemission. Indeed, the integrated spectral weight of the

incoherent background is proportional to $(1 - Z)$, Eq.(7). It turns out to be much larger than the coherent contribution, proportional to $Z \ll 1$. Finally, the \mathbf{k} dependent *incoherent* background might obscure the experimental determination of the Fermi-level crossing, leaving the ‘leading edge’ determination of it¹⁸ rather unreliable.

In the following we concentrate on the angular, spectral and polarisation dependence of the first coherent term, Eq.(9). The present experimental resolution⁴ allows probing of the intrinsic damping of the coherent polaron tunnelling. This damping appears due to the random field and low-frequency lattice and spin fluctuations described by the polaron self-energy $\Sigma_p(\mathbf{k}, E)$, so that the coherent part of the spectral function is given by

$$A_p(\mathbf{k}, E) = -(1/\pi) \frac{\Im \Sigma_p(\mathbf{k}, E)}{[E + \Re \Sigma_p(\mathbf{k}, E) - \xi_{\mathbf{k}}]^2 + [\Im \Sigma_p(\mathbf{k}, E)]^2}. \quad (11)$$

Hence, the theory of the narrow ARPES peak reduces to the determination of the self-energy of the coherent small hole polaron scattered by impurities, low-frequency deformation and spin fluctuations.

3. Self-energy of 1D hole in the non-crossing approximation

Due to energy conservation small polarons exist in the Bloch states at temperatures well below the optical phonon frequency $T \ll \omega/2$ no matter how strong their interaction with phonons is^{37,45–47,2}. This textbook result, known for a long time, has been questioned by some authors⁴⁸. It has been shown⁴⁹ that the confusion is due to a profound misunderstanding of the strong-coupling expansion by those authors. The finite polaron self-energy appears only due to the (quasi)elastic scattering. First we apply the simplest non-crossing (ladder) approximation to derive the analytical results, Fig.2. Within this approximation the self-energy is \mathbf{k} -independent for a short-range scattering potential like the deformation or a screened impurity potential, so that

$$\Sigma_p(E) \sim \sum_{\mathbf{k}} G_p^R(\mathbf{k}, E), \quad (12)$$

with $G_p^R(\mathbf{k}, E) = [E - \xi_{\mathbf{k}} - \Sigma_p(E)]^{-1}$

The oxygen polaron spectrum is parametrised in the tight-binding model as²⁶

$$\xi_{\mathbf{k}}^{x,y} = 2[t \cos(k_x, y a) - t' \cos(k_y, x a) + t_c \cos(k_z d)] - \mu, \quad (13)$$

If the oxygen hopping integrals in Eq.(13), reduced by the narrowing effect, are positive, the minima of the polaron bands are found at the Brillouin zone boundary in X $(\pi, 0)$ and Y $(0, \pi)$. The wave vectors corresponding to the energy minima belong to the stars with two prongs. Their group has only 1D representations. This means that the spectrum is degenerate with respect to

the number of prongs of the star. The spectrum Eq.(13) belongs to the star with two prongs, and, hence it is a two-fold degenerate³⁶. The doublet is degenerate if the hole resides on the apical oxygen⁵⁰. In general, the degeneracy can be removed due to the chains in the buffer layers of Y123 and Y124, so that the y -polaronic band corresponding to the tunneling along the chains might be the lowest one.

As mentioned above the oxygen hole is (quasi) one-dimensional due to a large difference between the oxygen hopping integrals for the orbitals elongated parallel to and perpendicular to the oxygen-oxygen hopping $t', t_c \ll t$. This allows us to apply a one-dimensional approximation, reducing Eq.(13) to two 1D parabolic bands near the X and Y points, $\xi_{\mathbf{k}}^{x,y} = k^2/2m^* - \mu$ with $m^* = 1/2ta^2$ and k taking relative to $(\pi, 0)$ and $(0, \pi)$, respectively. Then, the equation for the self-energy in the non-crossing approximation, Eq.(12) takes the following form

$$\Sigma_p(\epsilon) = -2^{-3/2} [\Sigma_p(\epsilon) - \epsilon]^{-1/2}, \quad (14)$$

for each doublet component. Here we introduce a dimensionless energy (and self-energy), $\epsilon \equiv (E + \mu)/\epsilon_0$ using $\epsilon_0 = (D^2 m^*)^{1/3}$ as the energy unit. The constant D is the second moment of the Gaussian white noise potential, comprising thermal and random fluctuations as $D = 2(V_0^2 T/M + n_{im} v^2)$, where V_0 is the amplitude of the deformation potential, M is the elastic modulus, n_{im} is the impurity density, and v is the coefficient of the δ -function impurity potential. The solution is

$$\Sigma_p(\epsilon) = \frac{\epsilon}{3} - \left(\frac{1 + i3^{1/2}}{2} \right) \left[\frac{1}{16} + \frac{\epsilon^3}{27} + \left(\frac{1}{256} + \frac{\epsilon^3}{216} \right)^{1/2} \right]^{1/3} - \left(\frac{1 - i3^{1/2}}{2} \right) \left[\frac{1}{16} + \frac{\epsilon^3}{27} - \left(\frac{1}{256} + \frac{\epsilon^3}{216} \right)^{1/2} \right]^{1/3}. \quad (15)$$

While the energy resolution in the present ARPES studies is almost perfect⁴, the momentum resolution remains rather poor, $\delta > 0.1\pi/a$. Hence we have to integrate the spectral function, Eq.(11), with a Gaussian momentum resolution to obtain the experimental photocurrent,

$$I(\mathbf{k}, E) \sim Z \int_{-\infty}^{\infty} dk' A_p(k', -E) \exp\left[-\frac{(k - k')^2}{\delta^2}\right]. \quad (16)$$

The integral is expressed in terms of $\Sigma_p(\epsilon)$, Eq.(15) and the tabulated Error function $w(z)$ as

$$I(\mathbf{k}, E) \sim -\frac{2Z}{\delta} \Im (\Sigma_p(\epsilon) [w(z_1) + w(z_2)]), \quad (17)$$

where $z_{1,2} = [\pm k - i/2\Sigma_p(\epsilon)]/\delta$, $w(z) = e^{-z^2} \operatorname{erfc}(-iz)$ and $\epsilon = (-E + \mu)/\epsilon_0$. This photocurrent is plotted as dashed lines in Fig.3 for two momenta, $k = 0.04\pi/a$ (almost Y or X points of the Brillouin zone) and $k = 0.3\pi/a$.

The chemical potential is placed in the charge transfer gap below the bottom of the hole band, $\mu = -20\text{meV}$, the momentum resolution is taken as $\delta = 0.28\pi/a$ and the damping $\epsilon_0 = 19\text{meV}$.

The imaginary part of the self-energy, Eq.(15) disappears below $\epsilon = -3/2^{5/3} \simeq -0.9449$. Hence this approximation gives a well-defined gap rather than a pseudogap. Actually, the non-crossing approximation fails to describe the localised states inside the gap (i.e. the Lifshitz tail of the density of states). One has to go beyond the simple ladder, Fig.2, to describe the single-electron tunnelling inside the gap³² and the ARPES spectra at very small binding energy.

4. Exact spectral function of 1D hole

The exact spectral function for a one dimensional particle in a random Gaussian white noise potential was derived by Halperin²⁷ and the density of states by Frisch and Lloyd⁵¹. Halperin derived two pairs of differential equations from whose solutions the spectral function of a ‘Schrodinger’ particle (i.e. in the effective mass approximation) and of a ‘discrete’ particle (tight-binding approximation) may be calculated. The QMC polaronic bandwidth is about 100 meV or larger³⁸, which allows us to apply the ‘Schrodinger’ particle spectral function, given by²⁷

$$A_p(k, \epsilon) = 4 \int_{-\infty}^{\infty} p_0(-z) \Re p_1(z) dz, \quad (18)$$

where $p_{0,1}(z)$ obey the two differential equations

$$\left[\frac{d^2}{dz^2} + \frac{d}{dz}(z^2 + 2\epsilon) \right] p_0 = 0, \quad (19)$$

and

$$\left[\frac{d^2}{dz^2} + \frac{d}{dz}(z^2 + 2\epsilon) - z - ik \right] p_1 + p_0 = 0, \quad (20)$$

with boundary conditions

$$\lim_{z \rightarrow \infty} z^{2-n} p_n(z) = \lim_{z \rightarrow -\infty} z^{2-n} p_n(z) \quad (21)$$

where k is measured in units of $k_0 = (D^{1/2}m^*)^{2/3}$. The first equation may be integrated to give

$$p_0(z) = \frac{\exp(-z^3/3 - 2z\epsilon) \int_{-\infty}^z \exp(u^3/3 + 2u\epsilon) du}{\pi^{1/2} \int_0^{\infty} u^{-1/2} \exp(-u^3/12 - 2u\epsilon) du}. \quad (22)$$

The equation for $p_1(z)$ has no known analytic solution, and hence must be solved numerically. There is however an asymptotic expression for $A_p(k, \epsilon)$ in the tail where $|\epsilon| \gg 1$:

$$A_p(k, \epsilon) \sim 2\pi(-2\epsilon)^{\frac{1}{2}} \exp\left[-\frac{4}{3}(-2\epsilon)^{\frac{3}{2}}\right] \cosh^2 \left[\frac{\pi k}{(-8\epsilon)^{\frac{1}{2}}} \right]. \quad (23)$$

In practice, for computational efficiency we use the exact spectral density for $-1.4 \leq \epsilon < 1$, and outside this range we use the asymptotic result for $\epsilon < -1.4$, Eq.(23) and the non-crossing approximation for $\epsilon \geq 1$, where they are almost indistinguishable from the exact result on the scale of the diagrams plotted here.

The result for $A_p(k, -E)$ integrated with the Gaussian momentum resolution is shown in Fig.3 for two values of the momentum (solid lines). Quite differently from the non-crossing approximation the exact spectral function (averaged with the momentum resolution function) has the Lifshitz tail due to the states localised by disorder within the normal state gap. However, besides this tail the non-crossing approximation gives very good agreement, and for binding energy greater than about 30meV it is practically exact.

The cumulative DOS

$$N_p(\epsilon) = (2\pi)^{-1} \int_{-\infty}^{\epsilon} d\epsilon' \int_{-\infty}^{\infty} dk A_p(k, \epsilon') \quad (24)$$

is expressed analytically⁵¹ in terms of the tabulated Airy functions $Ai(x)$ and $Bi(x)$ as

$$N_p(\epsilon) = \pi^{-2} [Ai^2(-2\epsilon) + Bi^2(-2\epsilon)]^{-1}. \quad (25)$$

The DOS $dN(\epsilon)/d\epsilon$ fits well the voltage-current tunnelling characteristics of cuprates³².

5. Theory of ARPES in Y124 and Y123

With the polaronic doublet, Eq.(13) placed above the chemical potential we can quantitatively describe high-resolution ARPES in Y123²¹ and Y124²⁰. First we explain the experimentally observed polarisation dependence of the intensity near Y and X²¹. The Bloch periodic function $u_{\mathbf{k}}(\mathbf{r})$ can be expressed in terms of the Wannier orbitals $w(\mathbf{r})$ as

$$u_{\mathbf{k}}(\mathbf{r}) = N^{-1/2} \sum_{\mathbf{m}} e^{i\mathbf{k} \cdot (\mathbf{m} - \mathbf{r})} w(\mathbf{r} - \mathbf{m}). \quad (26)$$

Then the dipole matrix element is given by the derivative of the Fourier component of the atomic (Wannier) orbital, $f_{\mathbf{k}} \equiv v_0^{-1/2} \int d\mathbf{r} w(\mathbf{r}) \exp(i\mathbf{k} \cdot \mathbf{r})$ as

$$\mathbf{d}(\mathbf{k}) = i(\mathbf{e} \cdot \nabla_{\mathbf{k}}) f_{\mathbf{k}}. \quad (27)$$

To estimate $f_{\mathbf{k}}$ we approximate the x, y oxygen orbitals contributing to the x and y polaronic bands, respectively, with $w_x(\mathbf{r}) = (1/8a_0^3\pi)^{1/2}(x/2a_0)\exp(-r/2a_0)$ and $w_y(\mathbf{r}) = (1/8a_0^3\pi)^{1/2}(y/2a_0)\exp(-r/2a_0)$. As a result we obtain for the x orbital,

$$\frac{\partial f_{\mathbf{k}}}{\partial k_x} = (8a_0^3\pi/v_0)^{1/2} a_0 \times \left[[(ka_0)^2 + 1/4]^{-3} - 6(k_x a_0)^2 [(ka_0)^2 + 1/4]^{-4} \right], \quad (28)$$

and

$$\frac{\partial f_{\mathbf{k}}}{\partial k_{y,z}} = -6(8a_0^3\pi/v_0)^{1/2} a_0^3 k_x k_{y,z} [(ka_0)^2 + 1/4]^{-4}, \quad (29)$$

Here \mathbf{k} is the photoelectron momentum and a_0 is the size of the Wannier function. For the case of y-orbital one should interchange x and y. Near the X and Y points of the Brillouin zone, $|k_{y,x}| \ll k$, respectively. Then it follows from Eq.(28) and Eq.(29) that the ARPES peak should be seen at X and almost disappear at Y if the photons are polarised along the x-direction, i.e. $\mathbf{e} \parallel \mathbf{a}$. If the polarisation is along the y-direction ($\mathbf{e} \parallel \mathbf{b}$) the peak appears at Y and almost disappears at X. Precisely this behaviour is observed in ARPES spectra obtained using polarised photons²¹, Fig.4. We also notice a very strong dependence of the dipole matrix element, Eq.(28) on the photon energy, $d \sim \nu^{-3}$ at large ν . Hence, it is not surprising if the ARPES peak disappears at large ν as has been recently observed⁵².

The exact 1D polaron spectral function, Eq.(18), integrated with the experimental momentum resolution, provides a quantitative fit to the ARPES spectra in Y124 along the $Y - \Gamma$ direction, as shown in Fig.5. The angular dispersion is described with the polaron mass $m^* = 9.9m_e$ in agreement with the Monte-Carlo calculations of the SFP mass³⁸. The spectral shape is reproduced well with $\epsilon_0 = 19meV$, Fig.6, in close agreement with the value of this parameter found in tunnelling experiments³². That yields an estimate of the polaron scattering rate, which appears to be smaller than the polaron bandwidth (about $100meV$ or larger), in agreement with the notion²⁶ that many high- T_c cuprates are in the clean limit. There is also quantitative agreement in the perpendicular direction $Y - S$, Fig.7, in a restricted region of small k_x , where almost no dispersion is observed around Y. Slight dispersion in the $Y - S$ direction towards the chemical potential might be due to a negative t' in Eq.(13).

However, there is a significant loss of the energy-integrated intensity along both directions, Fig. 8, which the theoretical spectral function alone cannot account for. The energy-integrated ARPES spectra obey the sum rule,

$$\int_{-\infty}^{\infty} dEI(\mathbf{k}, E) \sim |d(\mathbf{k})|^2 n_{\mathbf{k}}, \quad (30)$$

where $n_{\mathbf{k}} = \langle h_{\mathbf{k}} h_{\mathbf{k}}^\dagger \rangle$. If the dipole matrix element is almost k-independent and the chemical potential is pinned well inside the charge-transfer gap, so that $n_{\mathbf{k}} = 1$ this integral would be \mathbf{k} independent as well. This is not the case for Y124, no matter what the scanning direction is, Fig.8. Therefore, we have to conclude that either the dipole matrix element is \mathbf{k} dependent or (and) the oxygen band is strongly correlated (in the Mott-Hubbard sense). As we have mentioned above, the incoherent background of SFP is angle dependent as well, which might contribute to the intensity loss.

The rapid loss of the integrated intensity in the $Y - S$ direction was interpreted by Randeria and Campuzano¹⁸ as a Fermi-surface crossing. While a Fermi-surface crossing is not incompatible with our scenario (see Fig.1 in-

set), we do not believe that it has really been observed in Y124. First of all these authors suppressed a few experimental curves in the $Y - \Gamma$ direction, Fig.5, which prevented them from observing the intensity loss in this ‘dielectric’ direction, where there is obviously no Fermi-surface crossing. This loss of intensity along $Y - \Gamma$ tells us that the intensity loss might be due to the matrix element rather than to the Fermi-surface crossing in both directions. This is confirmed by our observation of a similar rapid loss of the intensity in a *dielectric*, FeSi²³, Fig.9 with no Fermi-surface at all. The peaks in the $Y - S$ direction are all 15 meV or more below the Fermi level - at a temperature of 1 meV, if the loss of spectral weight were due to a Fermi-surface crossing one would expect the peaks to approach much closer to the Fermi level. Also the experimental spectral shape of the intensity at $\mathbf{k} = \mathbf{k}_F$ is incompatible with any theoretical scenario, including different marginal Fermi-liquid models, Fig.10. The spectral function on the Fermi surface should be close to a simple Lorentzian,

$$A_p(\mathbf{k}_F, E) \sim \frac{|E|^\beta}{E^2 + \text{constant} \times E^{2\beta}}, \quad (31)$$

because the imaginary part of the self-energy behaves as $|E|^\beta$ with $0 \leq \beta \leq 2$. On the contrary, the experimental intensity shows a pronounced minimum at the alleged Fermi-surface, Fig.10.

If there is indeed no Fermi-surface crossing in many cuprates, as we argue, why then does the ‘maximum locus’ determination point to a large Fermi surface in cuprates, which is drastically incompatible with their kinetic and thermodynamic properties? We propose that it appears due to the fact that oxygen semiconducting band has its minima at large k inside or even on the boundary of the Brillouin zone. That is why ARPES show intense peaks near large \mathbf{k} imitating a large Fermi-surface.

6. Summary and conclusions

In summary, we have proposed a theory of ARPES in cuprates based on the LDA+U band structure and the bipolaron theory compatible with the normal state kinetic and thermodynamic properties of these materials. The theory explains the narrow flat bands observed in Y123 and Y124, including their polarisation, spectral and angular dependence, as well as a featureless (but dispersive) background. The ARPES peak originates from the hole excitations of the polaronic oxygen band of the buffer layers, in agreement with the experimental results and electronic structure of Schabel *et al*²¹. Differently from these authors we suggest that this band is intrinsic for cuprates and takes part in the bipolaron formation and superconductivity, which is nicely confirmed by a few independent studies⁵⁰. The normal state gap is half of the bipolaron binding energy. The angular dependence of the peak and of the gap is due to the polaron band dispersion, which agrees well with the QMC results for the small Fröhlich polaron.

The spectral shape of the peak is affected by the soft lattice, spin and random fluctuations. The characteristic

scattering rate agrees well with that found in the tunnelling experiments³². This scattering rate is temperature dependent not only due to the thermal lattice fluctuations, but also because of the anomalous screening below T_c in the charged Bose-liquid². The Bose-Einstein condensate screens effectively the long-range Coulomb potential of impurities. As a result one can expect a drastic change of the damping ϵ_0 when T_c is passed. That might help to understand the near disappearance of the narrow peak above T_c in some Bi-cuprates. On the other hand in the stoichiometric Y124 with (theoretically) no impurities, one can expect about the same results from ARPES below and above T_c , which seems to be the case²⁰. Within the bipolaron theory there is only one *single – particle* gap, which is half of the bipolaron binding energy both below and above T_c .

We believe that many cuprates are doped insulators with no Fermi surface at all due to the bipolaron formation. The Fermi-surface crossing, if it were firmly established in the overdoped samples, would correspond to a small Fermi surface of the oxygen band pockets located at finite \mathbf{k} like in many ordinary semiconductors, for example, in Ge and Si.

The authors greatly appreciate enlightening discussions with D.S. Dessau, N.E. Hussey, V.V. Kabanov, P.E. Kornilovitch, G.J. Kaye, A.I. Lichtenstein, G.A. Sawatzky, J.R. Schrieffer, Z.-X. Shen, J. Zaanen, G. Zhao, and R. Zeyher. C.J.D. has been supported in this work by a grant from the EPSRC of the UK.

-
- ¹ J.G. Bednorz and K.A. Müller, Z.Phys. B **64**, 189 (1986); Angew.Chem.Int.Ed.Engl. **27**, 735 (1988).
² A.S. Alexandrov and N.F. Mott, Rep. Prog. Phys. **57** 1197; ‘High Temperature Superconductors and Other Superfluids’ Taylor and Francis, London (1994); ‘Polarons and Bipolarons’, World Scientific, Singapore (1995).
³ A.S. Alexandrov, in ‘Models and Phenomenology for Conventional and High-temperature Superconductivity’ (Course CXXXVI of the International School of Physics ‘Enrico Fermi’), eds. G. Iadonisi, J.R. Schrieffer and M.L. Chiofalo, IOS Press (Amsterdam), p. 309 (1998).
⁴ for a recent review see Zhi-xun Shen, in ‘Models and Phenomenology for Conventional and High-temperature Superconductivity’ (Course CXXXVI of the International School of Physics ‘Enrico Fermi’), eds. G. Iadonisi, J.R. Schrieffer and M.L. Chiofalo, IOS Press (Amsterdam), p. 141 (1998).
⁵ D.C. Johnston, Phys. Rev. Lett. **62**, 957 (1989).
⁶ K.A. Müller *et al.*, J.Phys.: Condens. Matter **10**, L291 (1998).
⁷ D. Mihailović *et al.*, J. Superconductivity, **10**, 337 (1997).
⁸ J. Hofer *et al.*, Physica C **297**, 103 (1998).
⁹ B. Batlogg *et al.*, Physica C **135 – 140**, 130 (1994); H.Y. Hwang *et al.*, Phys. Rev. Lett. **72**, 2636 (1994)

- ¹⁰ J.W. Loram *et al.*, Physica C (Amsterdam), **235**, 134 (1994).
¹¹ C. Kendziora *et al.*, Phys. Rev. Lett. **79**, 4935 (1997).
¹² Z.-X. Shen and J.R. Schrieffer, Phys. Rev. Lett. **78**, 1771 (1997) and references therein.
¹³ Ch. Renner *et al.*, Phys. Rev. Lett. **80**, 149 (1998).
¹⁴ N.L. Saini *et al.*, Phys. Rev. Lett. **79**, 3467 (1997).
¹⁵ N.L. Saini *et al.*, Phys. Rev. Lett. **82**, 2619 (1999)
¹⁶ J.W. Loram *et al.*, J. of Superconductivity **7**, 243 (1994).
¹⁷ H. Ding *et al.*, Nature (London) **382**, 51 (1996).
¹⁸ M. Randeria and J.-C. Campuzano, in ‘Models and Phenomenology for Conventional and High-temperature Superconductivity’ (Course CXXXVI of the International School of Physics ‘Enrico Fermi’), eds. G. Iadonisi, J.R. Schrieffer and M.L. Chiofalo, IOS Press (Amsterdam), p. 115 (1998).
¹⁹ J. Mesot *et al.*, Phys. Rev. Lett. **82**, 2619 (1999).
²⁰ K. Gofron *et al.*, Phys. Rev. Lett. **73**, 3302 (1994).
²¹ M. C. Schabel *et al.*, Phys. Rev. B **57**, 6090 (1998).
²² A. Ino *et al.*, unpublished.
²³ C.-H. Park *et al.*, Phys. Rev. B **52**, R16981 (1995).
²⁴ A.S. Alexandrov, Philos. Trans. R. Soc. London, Ser. **A356**, 197 (1998).
²⁵ see in ‘Anharmonic Properties of High- T_c Cuprates’, eds. D. Mihailović, G. Ruani, E. Kaldis and K.A. Müller, World Scientific, Singapore (1995), and also in ‘Polarons and Bipolarons in High- T_c Superconductors and Related Materials’, eds. E.K.H. Salje, A.S. Alexandrov and W.Y. Liang, Cambridge University Press, Cambridge (1995).
²⁶ A.S. Alexandrov, Phys. Rev. B **53**, 2863 (1996).
²⁷ B.I. Halperin, Phys. Rev. **139**, A104 (1965).
²⁸ C.R.A. Catlow, M.S. Islam and X. Zhang, J. Phys.: Condens. Matter **10**, L49 (1998).
²⁹ A.S. Alexandrov, Physica C (Amsterdam) **182**, 327 (1991).
³⁰ A.S. Alexandrov, V.V. Kabanov and N.F. Mott, Phys. Rev. Lett. **77**, 4796 (1996).
³¹ A.S. Alexandrov and G.J. Kaye, J. Phys.: Condens. Matter **11**, L15 (1999).
³² A.S. Alexandrov, Physica C (Amsterdam) **305**, 46 (1998).
³³ G.A. Sawatzky, invited talk at the Rinberg Workshop (Rinberg Castle, Germany), April 1999.
³⁴ D.A. Wollman *et al.*, Phys. Rev. Lett. **71**, 2134 (1993); C.C. Tsuei *et al.*, Phys. Rev. Lett. **73**, 593 (1994); J.R. Kirtley *et al.*, Nature **373**, 225 (1995); C.C. Tsuei *et al.*, Science **272**, 329 (1996).
³⁵ A.S. Alexandrov, Phys. Rev. Lett. **82**, 2620 (1999).
³⁶ A.S. Alexandrov and V.V. Kabanov, Phys. Rev. B **59** (1999).
³⁷ I.G. Lang and Yu.A. Firsov, Zh.Eksp.Teor.Fiz. **43**, 1843 (1962) (Sov.Phys.JETP **16**, 1301 (1963)).
³⁸ A.S. Alexandrov and P.E. Kornilovich, Phys. Rev. Lett. **82**, 807 (1999).
³⁹ A.S. Alexandrov, Phys. Rev. B **46**, 2838 (1992).
⁴⁰ B.K. Chakraverty, J. Ranninger, and D. Feinberg. Phys. Rev. Lett. **82**, 2621 (1999).
⁴¹ A.S. Alexandrov and C. Sricheewin, unpublished.
⁴² G.J. Kaye, Phys. Rev. B **57**, 8759 (1998).
⁴³ Y. Okimoto *et al.*, Phys. Rev. Lett. **75**, 109 (1995); Y. Okimoto *et al.*, Phys. Rev. B **55**, 4206 (1997).
⁴⁴ D.S. Dessau *et al.*, Phys. Rev. Lett. **81**, 192 (1998).

- ⁴⁵ T. Holstein, *Ann.Phys.* **8**, 325-42; *ibid* p. 343 (1959).
- ⁴⁶ J. Appel, in *Solid State Physics*, eds. F. Seitz, D. Turnbull and H. Ehrenreich, Academic Press **21** (1968).
- ⁴⁷ Yu.A. Firsov (ed), *Polarons*, Nauka (Moscow) (1975).
- ⁴⁸ E.V.L. de Mello and J. Ranninger, *Phys. Rev.* **B55**, 14872 (1997); *ibid* **B58**, 9098 (1998).
- ⁴⁹ Yu.A. Firsov *et al*, *Phys. Rev. B* **59**, (1999).
- ⁵⁰ There is strong experimental evidence for apical holes in cuprates from the site-specific X-ray absorption (M. Merz *et al*, *Phys. Rev. Lett.* **80**, 5192 (1998)) and from the site-specific effect of Ba and Y substitution for Pr in $YBa_2Cu_3O_7$ (J.D. Dow, U. Howard and A. Blackstead, *Bulletin of American Physical Society*, **43**, 877 (1998)).
- ⁵¹ H.L. Frisch and S.P. Lloyd, *Phys. Rev.* **120**, 1175 (1960).
- ⁵² D.S. Dessau *et al*, *cond-mat/9904050*.

Figure Captures

Fig.1. Schematic LDU+U density of states. The chemical potential is pinned inside the charge transfer gap (a) due to the bipolaron formation in underdoped cuprates. It might enter the oxygen band in overdoped cuprates (b) if the polaron band crosses the bipolaron one (inset).

Fig.2. The non-crossing diagram for the self-energy. The dashed line corresponds to the random potential and (or) to the thermal lattice and spin fluctuations.

Fig.3. The polaron spectral function, integrated with the momentum resolution function for two angles, $k = 0.04\pi/a$ (upper curves), and $k = 0.30\pi/a$ with the damping $\epsilon_0 = 19meV$, the momentum resolution $\delta = 0.28\pi/a$ and the polaron mass $m^* = 9.9m_e$. The bipolaron binding energy $2|\mu| = 40meV$. The dashed curves are the spectral density integrated with the momentum resolution in the non-crossing approximation.

Fig.4. Polarisation dependence of the ARPES peak in $Y123^{21}$ near X and Y points.

Fig.5. Theoretical ARPES spectra (b) compared with experiment (a) in $Y124^{20}$ for $Y-\Gamma$ direction. Parameters are those of Fig.3.

Fig.6. Theoretical fit (dashed lines) to two experimental ARPES curves corresponding to $k = 0.04\pi/a$ (upper curves), and $k = 0.30\pi/a$.

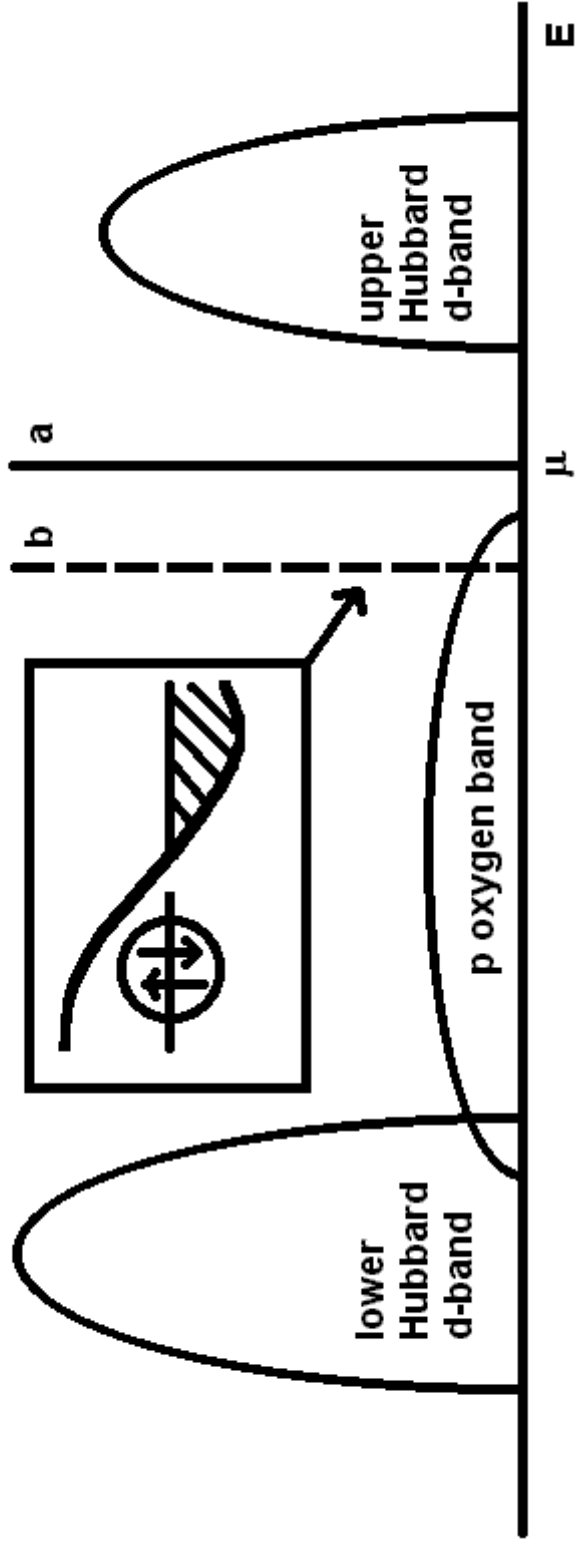
Fig.7. Theoretical ARPES spectra (b) compared with experiment (a) in $Y124^{20}$ for $Y-S$ direction.

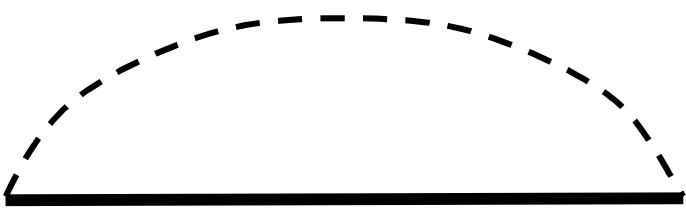
Fig.8. The energy-integrated ARPES intensity in $Y124$ in the $Y-\Gamma$ (a) and $Y-S$ (b) directions. Momenta are measured relative to the Y-point of the Brillouin zone.

Fig.9. (a) The energy-integrated ARPES intensity in $FeSi^{23}$ as a function of the analyser angle. The spectra are shown in (b).

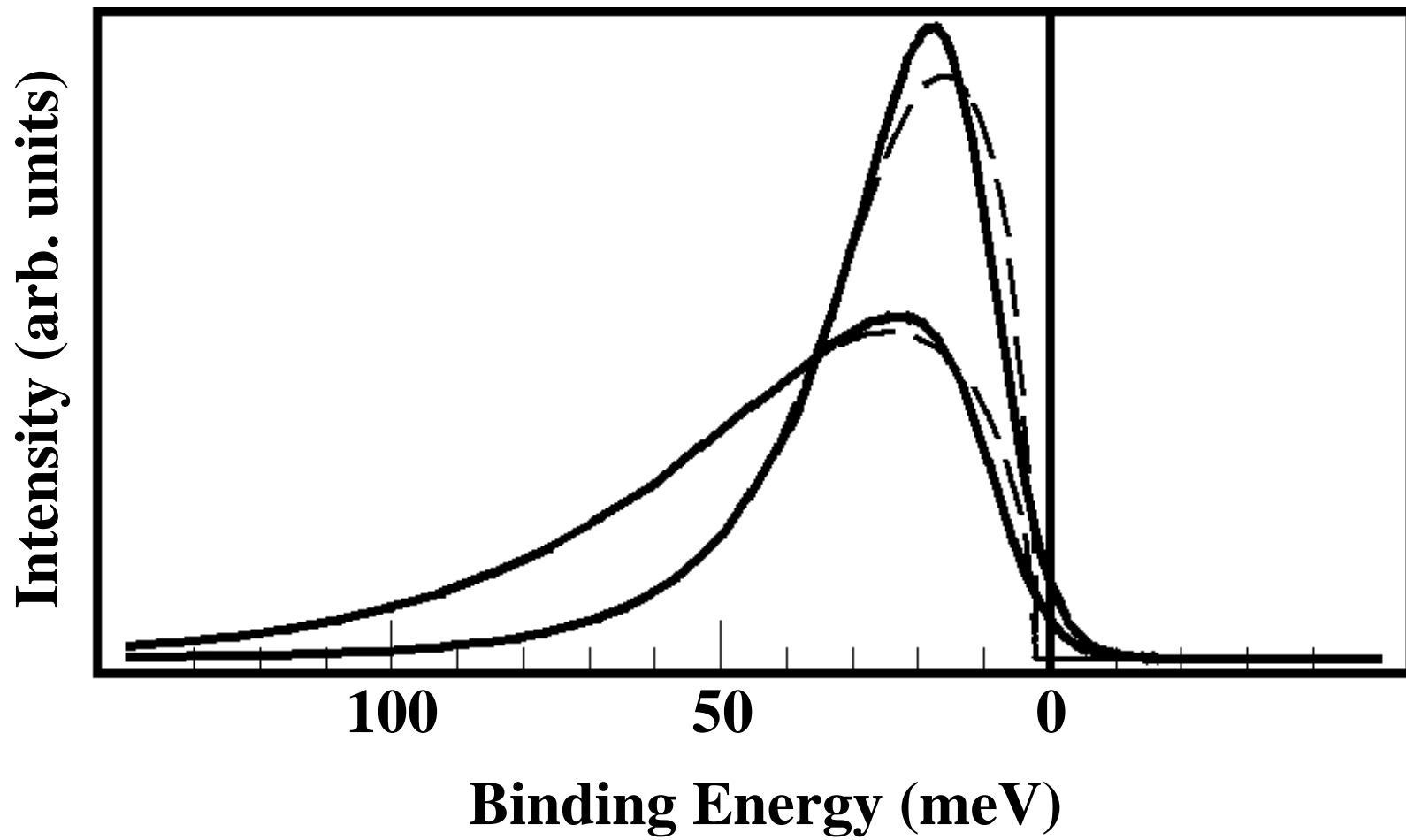
Fig.10. The experimental ARPES signal (solid line) on the alleged Fermi-surface does not correspond to a Fermi-liquid spectral function (dashed line). We assume particle-hole symmetry to obtain the spectral function for negative binding energy.

LDA+U DOS



$$\Sigma(E) = \int_{\text{G}(k, E)}$$


The diagram shows a contour in the complex plane. The real axis is represented by a solid black horizontal line. Above it, a dashed black semi-circular arc connects the two ends of the real axis. Below the real axis, the text $G(k, E)$ is centered.



Theory

Experiment

